

Wave-number domain analysis for determining the response of linear space-invariant time-varying systems

Wending Mai ^{*}, Jingwei Xu , Arkaprovo Das, and Douglas H. Werner

Electrical Engineering Department, the Pennsylvania State University, University Park, Pennsylvania 16802, USA



(Received 30 August 2023; accepted 15 September 2023; published 9 October 2023)

System response analysis is a powerful method for analyzing linear time-invariant (LTI) systems. In this work, we have demonstrated that a system response approach can also be applied to analyze the so-called linear space-invariant (LSI) but time-varying problems, which represent a dual of the conventional LTI problems. In this proposed approach, we perform a Fourier transform of the electric field distribution on the space coordinate, rather than in time, and express it in the wave-number domain. Specifically, we express any input signal and its corresponding output in the wave-number domain. Then, the transfer function for the LSI time-varying system can be extracted as a one-time computation by evaluating the ratio of the output signal to the input signal in the wave-number domain. Once the transfer function is extracted, the output response to any input with an arbitrary temporal profile can be computed instantaneously. Furthermore, for a system with a complicated temporal profile, the proposed method allows us to decompose it into several simpler subsystems that appear sequentially in time. The transfer function of that complicated system can be expressed as the product of those of the individual subsystems, such that it can be evaluated more efficiently.

DOI: [10.1103/PhysRevA.108.043504](https://doi.org/10.1103/PhysRevA.108.043504)

I. INTRODUCTION

As an emerging field, time-varying metamaterials have attracted the attention of researchers over the past several years. This is primarily because they provide an additional degree of freedom to control electromagnetic (EM) wave propagation [1–6]. For example, there exists a class of problems where EM waves propagate in an infinite and homogeneous medium whose permittivity or permeability can change with time. This topic was explored by Morganthaler in the 1950s [7]. More recently, some researchers have introduced the concept of a “temporal boundary” [8], which has been explored both theoretically and numerically. Applications of temporal boundaries include temporal effective media [9], temporal coatings [10,11], temporal aiming [12], polarization conversion [13], energy pumping [14], photonic time crystals [15,16], and so on [17–20]. We refer to this class of problems as linear space-invariant (LSI) systems, which serve as a dual of the conventional linear time-invariant (LTI) systems where the material properties vary spatially.

In order to analyze LSI systems, researchers have proposed several analytical formalisms, such as temporal transfer matrix methods (TTMMs) [19,21] and d’Alembert’s formula [22]. These methods rely on solving temporal boundary conditions at the time instances when the material properties change abruptly. If the medium’s permittivity is gradually varying in time, these methods could be cumbersome. Other researchers have proposed solutions to waves propagating in a continuously changing media using the well-known Wentzel-Kramers-Brillouin (WKB) method [23]. However,

this technique is intrinsically approximate and may not be accurate in many cases. Other researchers have developed closed-form solutions to the wave equations for some special cases of the materials system’s temporal profile [24]. However, to this day, a systematic solution strategy for general LSI problems remains unavailable.

In light of the shortcomings of the above-mentioned theoretical works, in this paper, we propose a general analysis method to determine the system response. By retrieving the transfer function of the LSI system from only one set of test inputs and the corresponding output signals (via simulation or measurement), the response to any arbitrary input can be efficiently determined. This transfer function computation represents a one-time exercise that is performed using numerical simulation tools or measurements. Once extracted, the output response can be obtained in real time for any arbitrary changes to the input profile, without requiring any further simulations or measurements. The proposed method can be especially useful whenever the detailed properties of the structure are not known, or when we simply want to treat the analyzed system as a black box. Section II introduces the proposed system analysis method and presents the corresponding design procedure. In Sec. III, we apply this approach to several scenarios with different temporal material profiles.

II. FORMALISM

To demonstrate the design procedure, first, let us consider a one-dimensional (1D) harmonic wave with an electric field given by $E(x, t) = E_0 e^{i(kx - \omega t + \phi)}$, where k is the wave number, ω is the angular frequency, and ϕ is the phase constant. The EM wave varies in both space and time, as illustrated in Fig. 1. The electric field can be projected as a curve varying in time

^{*}Corresponding author: wdm@ieee.org

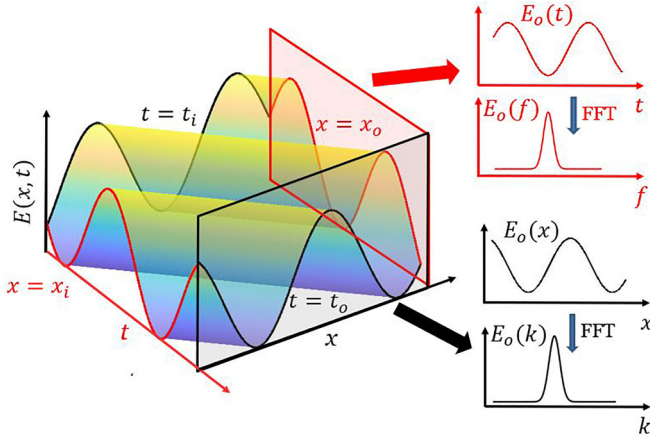


FIG. 1. Representation of an EM wave in the space-time domain. To investigate conventional LTI systems, researchers usually capture the field at specific locations x_i, x_o , which varies in time (red curves), then transform it into the frequency domain. For LSI systems, we propose to capture the field at specific times t_i, t_o , which varies in space, and then study its properties in the wave-number domain (the subscripts i and o denote input and output respectively).

at a specific location (red), or it can be projected as a curve varying in space at a specific time (black).

For conventional LTI problems, a Fourier transform is performed on the time coordinate and the resultant relationship is provided in Eq. (1). The input (at $x = x_i$) and output (at $x = x_o$) curves can be transformed into the frequency domain as $E_i(\omega)$ and $E_o(\omega)$, respectively. These parameters are related to the system transfer function $S(\omega)$ in the frequency domain by

$$E_o(\omega) = S(\omega)E_i(\omega). \quad (1)$$

On the other hand, in LSI systems, the spectral content of the wave may be altered as it propagates in a time-varying medium. Therefore, Eq. (1) becomes ill-defined because the input at a certain frequency would not necessarily trigger a response at the same frequency. However, the wave number in such systems remains invariant. Therefore, it is instructive to perform a Fourier transform of the electric fields on the spatial coordinates:

$$E(k, t) = \int_{-\infty}^{\infty} E(x, t) e^{-2\pi i k x} dx. \quad (2)$$

Given a test input at $t = t_i$ (E_{ti}), the LSI system under investigation generates an output at $t = t_o$ (E_{to}), and the transfer function can be derived in a way similar to that of conventional LTI systems [25]:

$$S(k) = \frac{E_{to}(k)}{E_{ti}(k)}. \quad (3)$$

It is worthwhile to note that, in order to retrieve the system transfer function in Eq. (3), only the input and output electric field are needed. Therefore, by measuring these quantities, the transfer function can be obtained even if the detailed properties of the structure are unknown. With the transfer function $S(k)$ computed, the output $E_o(k)$ for any arbitrary input $E_i(k)$

can be efficiently calculated at $t = t_o$ as

$$E_o(k) = S(k)E_i(k). \quad (4)$$

It should be noted that the bandwidth of the input would decide the effective wave-number range of the transfer function $S(k)$. We refer to this range as the bandwidth of the transfer function in the following discussion. Here we define the bandwidth of the test input using the -3 -dB points where the wave energy is half of its maximal value. Importantly, the transfer function calculated by Eq. (3) is valid only over this wave-number range.

III. EXAMPLES

In order to prove the effectiveness of the proposed method, we apply it to several LSI systems, and compare the results with simulations for validation. The various steps of the entire process are outlined in Fig. 2. First, we conduct a test process (the first row with the blue background) to obtain the transfer function (the second row with the orange background) using Eq. (3). Next, we apply the transfer function to a different input, which we refer to as the ‘‘application input.’’ Then the output can be computed by using Eq. (4) (the third row with the white background).

For better comparison, both the test input [$E_{ti}(x)$] and application input [$E_i(x)$] are set to be of the same form for all examples considered here. In particular, the field is defined in the spatial domain at $t_i = 0$ using a modulated Gaussian pulse:

$$E(x) = -\exp\left[\frac{-4\pi(x-x_0)^2}{x_n^2}\right] \cos[k_0 x], \quad (5)$$

where x_0 denotes the reference point, x_n is a parameter that determines the bandwidth, and k_0 is the center wave number of the modulated signal. In this paper, k_0 is set to 1.05×10^7 1/m (wavelength $\lambda_0 = 600$ nm), which corresponds to a period $T_0 = 4$ fs in free space. To obtain a system response that is valid over a broadband regime, we choose a relatively small value of x_n ($3.33\lambda_0$). The test input and its Fourier transform are shown in Figs. 2(a) and 2(b), respectively, where the green block indicates the corresponding effective bandwidth.

As for the application input, it can be arbitrarily chosen in the ideal case. However, to ensure that the input lies inside the effective bandwidth of the transfer function, we used the modulated Gaussian pulse defined in Eq. (5), but with a narrower bandwidth ($x_n = 16.67\lambda_0$). The application input and its Fourier transform are shown in Figs. 2(h) and 2(i) respectively. In practice, the Fourier transform in Eq. (2) is calculated using a discrete Fourier transform (DFT). So, Eq. (2) may be rewritten in terms of a DFT expression as

$$E(k, t) = \sum_{n=0}^{N-1} E(x, t) e^{-2\pi i k n \Delta x / N}, \quad (6)$$

where $x = n\Delta x$, and Δx is the mesh element size.

A. A single temporal boundary

First, we investigate a simple system where there is only a single temporal boundary, denoted as S1. The temporal boundary is set at $t_1 = 60T_0$ when the relative permittivity

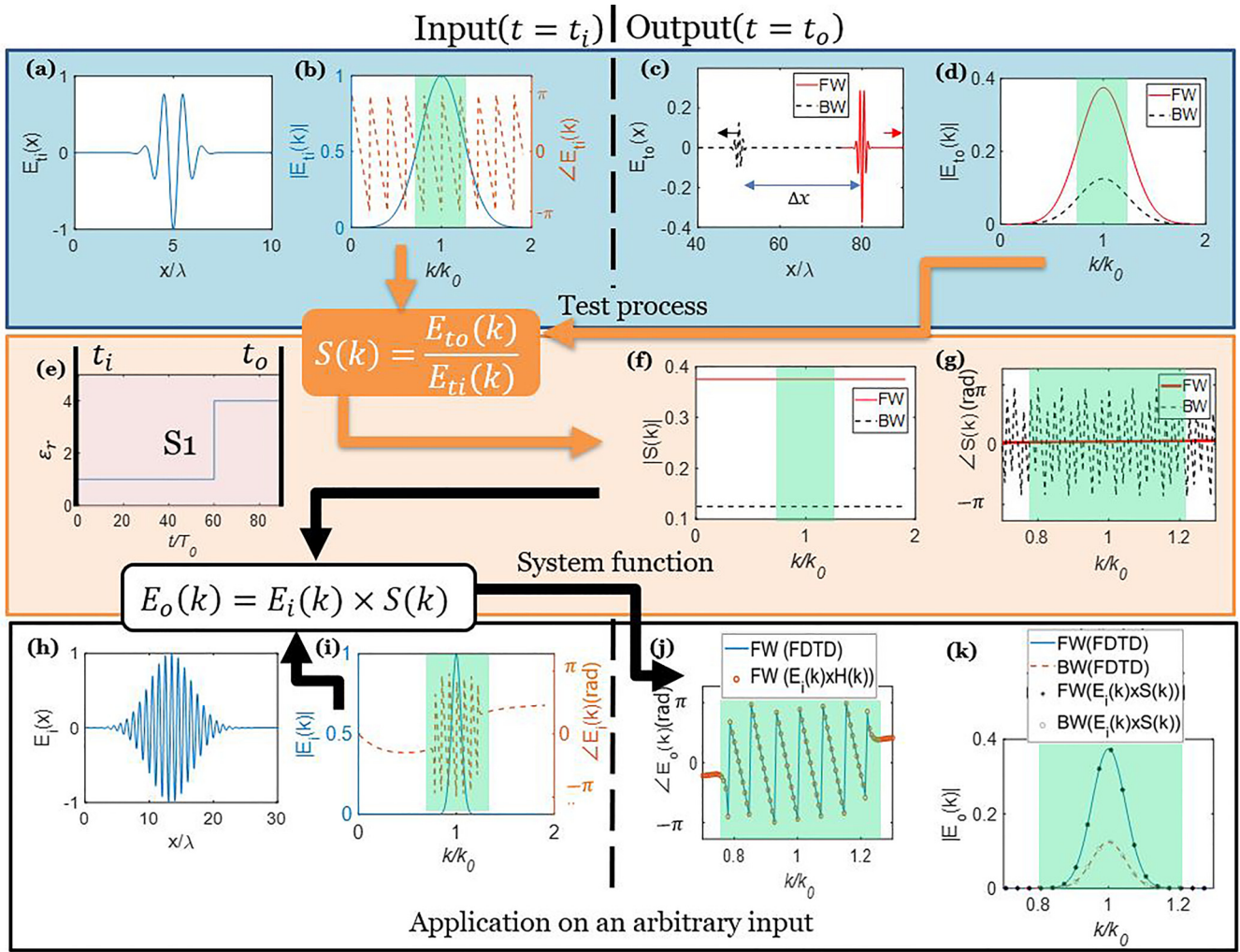


FIG. 2. The system response analysis considered in Sec. III A 1. A temporal system with a single temporal boundary (the FW and BW terms are decoupled). The magnitude of the electric field is normalized to that of the input. This figure shows the test process (blue background) to obtain the transfer function (orange background) and the application to a different input (white background). (a) The test input in the spatial and (b) wave-number domains, where the bandwidth of the input is indicated by a green block. (c) The output corresponding to a test input in the spatial and (d) wave-number domains. (e) The temporal profile of the permittivity. (f) The magnitude and (g) phase of the retrieved transfer function. The application input in the (h) spatial and (i) wave-number domains. (j) The phase and (k) the normalized magnitude of the output calculated using the proposed method and FDTD simulations.

ϵ_r of the medium changes abruptly from 1 to 4, as shown in Fig. 2(e). The output field is captured at a time $t_o = 90T_0$ (E_{t_o}), which can be computed using an finite-difference time-domain (FDTD) method as depicted in Fig. 2(c). As can be seen, the output curve is composed of a forward (FW) and a backward (BW) term, which propagate in opposite directions. We studied two different subcases depending on whether the FW and BW terms are considered separately or together.

1. FW and BW terms decoupled

After decoupling E_{t_o} into FW (E_{t_o-fw}) and BW (E_{t_o-bw}) terms, we evaluate their Fourier transforms in the wave-number domain, which are shown in Fig. 2(d). Applying Eq. (3), the transfer function can be calculated as $S_{fw}(k) = E_{t_o-fw}(k)/E_{t_i}(k)$ and $S_{bw}(k) = E_{t_o-bw}(k)/E_{t_i}(k)$ for the FW and BW terms, respectively. The magnitudes and phases of

$S_{fw}(k)$ and $S_{bw}(k)$ are plotted in Figs. 2(f) and 2(g) respectively. It can be observed that their magnitudes are constant over the entire bandwidth. This is as expected since the dispersion of the medium is not considered. Moreover, their magnitudes are numerically equal to the reflection and transmission coefficients, which match well with the theoretical results [7,8].

As for the phase plot shown in Fig. 2(g), we know from Eq. (3) that the phase of the transfer function corresponds to the phase difference between the output and input. For the FW term, the phase is identical to that of the input, therefore, $\angle S_{fw}(k) = 0$. On the other hand, as shown in Fig. 2(c), at time t_o , the BW term maintains a constant spatial distance Δx with respect to the FW term, which leads to a phase difference between the FW and BW terms that can be represented as

$$\varphi(k) = k\Delta x. \quad (7)$$

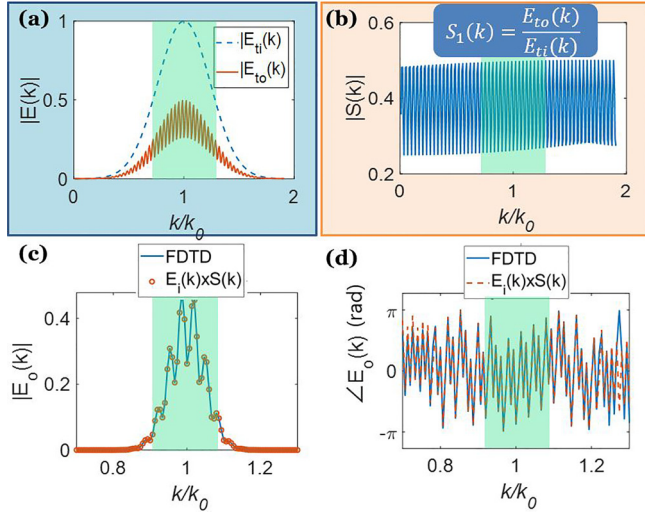


FIG. 3. System response analysis for example considered in Sec. III A 2. A single temporal boundary with the FW and BW terms considered together. The magnitude of the electric field is normalized to that of the input. The temporal profile, as well as t_i and t_o , is the same as used in Sec. III A 1 [Fig. 2(e)]. (a) Magnitude of the test input and total output in the wave-number domain. (b) Magnitude of the transfer function $S_1(k)$. (c) Magnitude and (d) phase of the total output corresponding to the application input determined using the proposed method and FDTD simulations. Notice that the application input is normalized.

Therefore, the phase difference between the BW term and the input is also k dependent [Eq. (7)], which leads to the oscillations in $\angle S_{bw}(k)$ [black curve in Fig. 2(g)].

Once the transfer function is extracted, we now excite this LSI system with an arbitrary application input and compute its output using the retrieved transfer function. The corresponding Fourier transform $E_i(k)$ is shown in Fig. 2(i). By multiplying $E_i(k)$ with the obtained transfer functions $S_{fw}(k)$ and $S_{bw}(k)$, the output in the wave-number domain $E_o(k)$ can be computed. The associated phases and magnitudes are plotted in Figs. 2(j) and 2(k) respectively. The results from the theory agree well with the simulations within the effective bandwidth of the transfer function.

2. FW and BW terms coupled

In some scenarios, if Δx is comparable to or smaller than the pulse length, then the FW and the BW terms of the output may overlap in space and cannot be decoupled easily. Therefore, it is instructive to investigate the “total” test output by adding the FW and BW terms in Fig. 2(c). The Fourier transform of the total output and test input is shown in Fig. 3(a). Similarly, the transfer function can be obtained by Eq. (3), whose magnitude is plotted in Fig. 3(b). The plot reveals significant ripples because the phase difference between the FW and BW terms is k dependent, as explained above. Therefore, this phase difference leads to the oscillatory features in the curves of both the test output [Fig. 3(a)] and the transfer function [Fig. 3(b)].

Next, we utilize this transfer function together with the application input. Figures 3(c) and 3(d) compare the magnitude

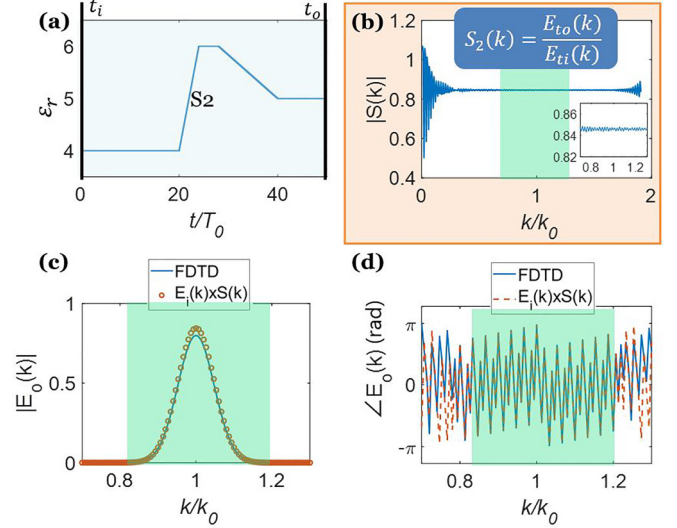


FIG. 4. System response analysis for example considered in Sec. III B. Medium with gradually changing permittivity. The magnitude of the electric field is normalized to that of the input. (a) The temporal profile of the permittivity. (b) The transfer function. (c) The magnitude and (d) phase of the output determined using the proposed method and FDTD simulations. Notice that the application input is normalized.

and phase of the output obtained using the proposed method as compared against FDTD simulations. The results demonstrate good agreement within the effective bandwidth of the transfer function.

B. Gradually changing material properties

It is worth mentioning that this method is not limited to temporal boundary problems, but also works for systems where the material properties (such as permittivity) change gradually. The temporal system under investigation here, denoted as S_2 , has the temporal permittivity profile shown in Fig. 4(a). The output field is captured at $t_o = 50T_0$. Overall, a gradually changing permittivity tends to produce very small BW terms when compared to the temporal boundary cases. Therefore, the curve of the transfer function is much smoother within the effective bandwidth, as seen in Fig. 4(b). The quantity $|S(k)|$ is nearly constant within the effective bandwidth, with a value around $|S(k_0)| = 0.84$. This makes sense physically because the medium’s permittivity is higher at t_o than it is at t_i . To keep the D field constant in time, the magnitude of the E field must necessarily decrease [Fig. 3(c)]. One interesting observation is that, although there is nearly no reflection, $S(k_0)$ is smaller than unity. This does not violate conservation of energy because time-varying media require an energy exchange with external sources [11,14].

At this point in the process, we again employ the application input together with the extracted transfer function. The calculated output correlates well with that obtained from the FDTD simulations, as compared in Figs. 4(c) and 4(d). However, some differences can still be observed because of numerical error. In general, adopting a finer mesh or using a higher order basis, namely h or p refinement, will lead to greater accuracy for the numerical simulation [26].

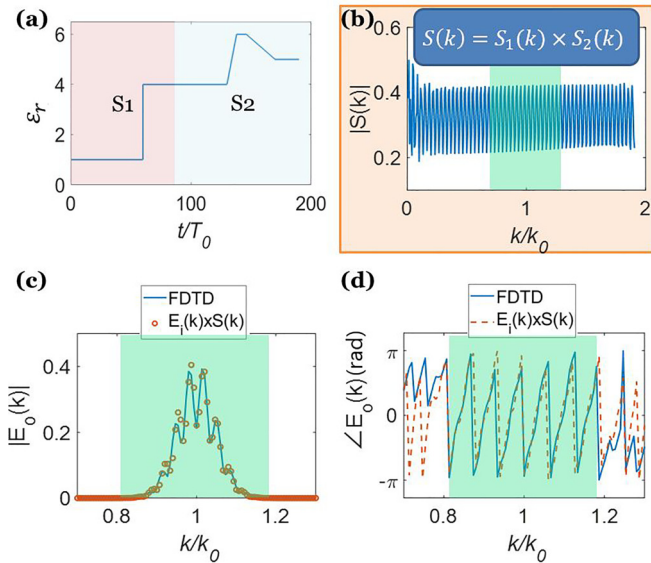


FIG. 5. System response analysis of the example considered in Sec. III C. A temporally cascaded system. The magnitude of the electric field is normalized to that of the input. (a) The permittivity profile of the system which is decomposed into two subsystems. (b) The total transfer function calculated by multiplying those of the two subsystems. (c) The amplitude and (d) phase of the output determined using the proposed method and FDTD simulations.

C. Cascading systems

One of the biggest advantages of the proposed approach is that it can be easily generalized to cascading systems. If N subsystems are “cascaded” (i.e., they appear in sequence in time), the total system response can be expressed as

$$S_{\text{total}}(k) = \prod_{i=1}^N S_i(k), \quad (8)$$

where $S_i(k)$ is the transfer function of the i th subsystem. It should be noted that in Eq. (8), it is assumed that the reflection of each subsystem can be ignored. As an example, we consider a system composed of two cascaded subsystems: S_1 and S_2 , which are the same as those considered in Secs. III A and III B, respectively. The permittivity profile of the entire system is depicted in Fig. 5(a). Its transfer function $S_{\text{total}}(k)$ is calculated as $S_1(k) \times S_2(k)$ which is plotted in Fig. 5(b). Figures 5(c) and 5(d) compare the magnitudes and phases of the output determined from the proposed method and FDTD simulations, respectively. The results agree well over the effective bandwidth, where the small discrepancies are due to numerical errors in the FDTD method. This example demonstrates that the response of a complex temporal system can be investigated by decomposing it into multiple relatively simpler subsystems. Comparing the examples considered in Secs. III A 2, III B, and III C [Figs. 3(b), 4(b), and 5(b)], we can observe that it is the abrupt change of permittivity that led to the fluctuations in the curve of $|S(k)|$, while the gradual change of permittivity only modulates its “overall” magnitude.

IV. CONCLUSION

In this paper, we propose a general system response analysis technique to address LSI problems in the wave-number domain. The transfer function of an LSI system can be retrieved from one set of test procedures, either numerically or experimentally. Once the transfer function is determined, the output due to any arbitrary input can be easily found. The validity of the formalism is guaranteed by the fact that wave number, instead of frequency, is constant in LSI systems. Importantly, the testing process can be conducted either numerically, based on simulations, or experimentally by utilizing measurements. Compared to other similar tools such as TTMMs, this method does not rely on a preknowledge of the detailed property of the structure and is ideally suited to black-box problems. This significantly broadens the capabilities of current theoretical approaches that have been reported in the literature. Furthermore, the transfer function of a cascaded structure can be derived simply by multiplying those of each subsystem. This aids in the analysis of complicated temporal systems by allowing them to be decomposed into a series of simpler ones. To this end, our systematic methodology is expected to greatly facilitate future research on LSI systems. Moreover, it can serve as a powerful tool for the analysis of all LSI problems, analogous to the well-established frequency domain techniques for their LTI counterparts.

Data underlying the results presented in this paper are not publicly available at this time but may be obtained from the authors upon reasonable request.

ACKNOWLEDGMENT

We acknowledge funding from the DARPA/DSO Extreme Optics and Imaging (EXTREME) Program (Grant No. HR00111720032).

The authors declare no conflicts of interest.

APPENDIX: SUPPLEMENTAL FIGURES FOR CASES CONSIDERED IN SEC. III

Figure 6 shows a supplemental figure of a single temporal boundary (FW and BW decoupled), Fig. 7 shows a supplemental figure of gradually changing material properties, and Fig. 8 shows a supplemental figure of a cascading system.

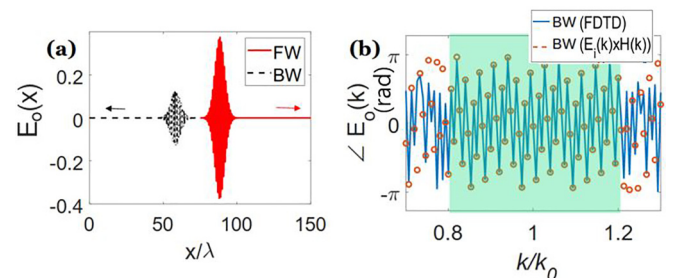


FIG. 6. (a) The output of the application process in the spatial domain [note that the corresponding input is shown in Fig. 2(h), and the Fourier transform of this plot is provided in Fig. 2(k)]. (b) The phase of the backward wave (BW) determined using the proposed method and FDTD simulations [Fig. 2(j) in the main text shows the phase of the forward (FW) wave]. The magnitude of the electric field is normalized to that of the input.

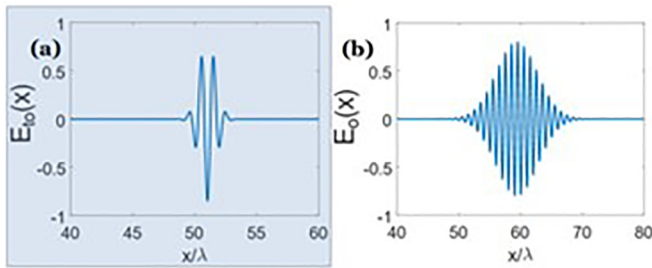


FIG. 7. The output of the (a) test and (b) application process in the spatial domain. Comparing the test output in Fig. S2(a) and the test input in Fig. 2(a), it can be seen that this system is reflectionless. Notice that the Fourier transform of Fig. S2(b) is actually the result shown in Fig. 4(c). The magnitude of the electric field is normalized to that of the input.

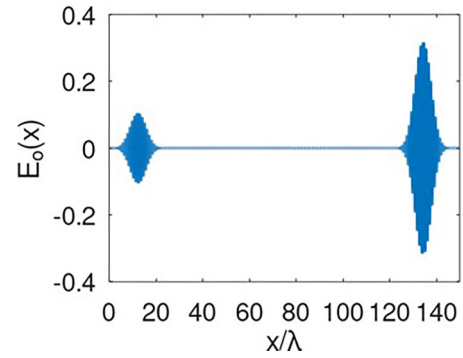


FIG. 8. The output of the application process in the spatial domain. Note that there is no test process here [compared to the case shown in Fig. S2(a)]. This is because the transfer function is calculated by multiplying those of the two subsystems [Eq. (6) in the main text], rather than retrieved by simulation. The magnitude of the electric field is normalized to that of the input.

- [1] N. Engheta, Metamaterials with high degrees of freedom: Space, time, and more, *Nanophotonics* **10**, 639 (2020).
- [2] D. Holberg and K. Kunz, Parametric properties of fields in a slab of time-varying permittivity, *IEEE Trans. Antennas Propag.* **14**, 183 (1966).
- [3] X. Guo, Y. Ding, Y. Duan, and X. Ni, Nonreciprocal metasurface with space-time phase modulation, *Light Sci. Appl.* **8**, 123 (2019).
- [4] L. Zhang, X. Q. Chen, R. W. Shao, J. Y. Dai, Q. Cheng, G. Castaldi, V. Galdi, and T. J. Cui, Breaking reciprocity with space-time-coding digital metasurfaces, *Adv. Mater.* **31**, 1904069 (2019).
- [5] A. Nagulu, T. Dinc, Z. Xiao, M. Tymchenko, D. L. Sounas, A. Alu, and H. Krishnaswamy, Nonreciprocal components based on switched transmission lines, *IEEE Trans. Microw. Theory Technol.* **66**, 4706 (2018).
- [6] S. Taravati, N. Chamanara, and C. Caloz, Nonreciprocal electromagnetic scattering from a periodically space-time modulated slab and application to a quasisonic isolator, *Phys. Rev. B* **96**, 165144 (2017).
- [7] F. R. Morgenthaler, Velocity modulation of electromagnetic waves, *IRE Trans. Microwave Theory Tech.* **6**, 167 (1958).
- [8] Y. Xiao, D. N. Maywar, and G. P. Agrawal, Reflection and transmission of electromagnetic waves at a temporal boundary, *Opt. Lett.* **39**, 574 (2014).
- [9] V. Pacheco-Peña and N. Engheta, Effective medium concept in temporal metamaterials, *Nanophotonics* **9**, 379 (2020).
- [10] V. Pacheco-Peña and N. Engheta, Antireflection temporal coatings, *Optica* **7**, 323 (2020).
- [11] W. Mai, J. Xu, and D. H. Werner, Antireflection temporal coatings: Comment, *Optica* **8**, 824 (2021).
- [12] V. Pacheco-Peña and N. Engheta, Temporal aiming, *Light Sci. Appl.* **9**, 129 (2020).
- [13] J. Xu, W. Mai, and D. H. Werner, Complete polarization conversion using anisotropic temporal slabs, *Opt. Lett.* **46**, 1373 (2021).
- [14] W. Mai, J. Xu, and D. H. Werner, Temporal multi-stage energy pumping, *Opt. Lett.* **47**, 2494 (2022).
- [15] E. Lustig, Y. Sharabi, and M. Segev, Topological aspects of photonic time crystals, *Optica* **5**, 1390 (2018).
- [16] Y. Sharabi, E. Lustig, and M. Segev, Disordered photonic time crystals, *Phys. Rev. Lett.* **126**, 163902 (2021).
- [17] J. Kim, D. Lee, S. Yu *et al.*, Unidirectional scattering with spatial homogeneity using correlated photonic time disorder, *Nat. Phys.* **19**, 726 (2023).
- [18] L. Yuan, Y. Shi, and S. Fan, Photonic gauge potential in a system with a synthetic frequency dimension, *Opt. Lett.* **41**, 741 (2016).
- [19] D. Ramaccia, A. Alù, A. Toscano, and F. Bilotti, Temporal multilayer structures for designing higher-order transfer functions using time-varying metamaterials, *Appl. Phys. Lett.* **118**, 101901 (2021).
- [20] D. Ramaccia, A. Toscano, and F. Bilotti, Light propagation through metamaterial temporal slabs: Reflection, refraction, and special cases, *Opt. Lett.* **45**, 5836 (2020).
- [21] J. Xu, W. Mai, and D. H. Werner, Generalized temporal transfer matrix method: A systematic approach to solving electromagnetic wave scattering in temporally stratified structures, *Nanophotonics* **11**, 1309 (2022).
- [22] W. Mai and D. H. Werner, Analytical transient analysis of temporal boundary value problems using the d'Alembert formula, *Opt. Lett.* **46**, 5727 (2021).
- [23] M. Chegnizadeh, K. Mehrany, and M. Memarian, General solution to wave propagation in media undergoing arbitrary transient or periodic temporal variations of permittivity, *J. Opt. Soc. Am. B* **35**, 2923 (2018).

- [24] A. G. Hayrapetyan, J. B. Götze, K. K. Grigoryan, S. Fritzsche, and R. G. Petrosyan, Electromagnetic wave propagation in spatially homogeneous yet smoothly time-varying dielectric media, *J. Quant. Spectrosc. Radiat. Transf.* **178**, 158 (2016).
- [25] A. Oppenheim and A. Willsky, *Signals and Systems* (Prentice-Hall, Englewood Cliffs, NJ, 1997).
- [26] S. McFee and D. Giannacopoulos, Optimal discretizations in adaptive finite element electromagnetics, *Int. J. Numer. Methods Eng.* **52**, 939 (2001).